energies

MDPI

Article

Research on Vehicle-to-Vehicle MIMO Wireless Channels in Various Tunnels

Jie Zhou [1], Sujie Wu [1], Zhikang Lv [1], Hong Luo [1], Ting Liu [1,2,*] and Genfu Shao [3]

[1] Department of Electronic and Electrical Engineering, Nanjing University of Information Science and Technology, Nanjing 210044, China; zhoujie@nuist.edu.cn (J.Z.); wusujie@126.com (S.W.); 1002rookie@sina.com (Z.L.); luohong@nuist.edu.cn (H.L.)
[2] National Mobile Communications Research Laboratory, Southeast University, Nanjing 210096, China
[3] College of Communication Engineering, Hangzhou Dianzi University, Hangzhou 310018, China; sgf@hdu.edu.cn
* Correspondence: liuting@nuist.edu.cn

Abstract: In this paper, we propose a geometry-based channel model for multiple-input multiple-output (MIMO) vehicle-to-vehicle (V2V) communications in practical tunnel scenarios. In the proposed channel model, the waves transmitted from the transmitter experience line-of-sight (LoS) and non-LoS (NLoS) before arriving at the receiver. The time-varying parameters of the propagation paths and angles are derived to characterize the channel non-stationarity. Furthermore, we derive the correlation property functions of the proposed V2V channel model; they are space cross-correlation functions (CCFs), temporal auto-correlation functions (ACFs), frequency CCFs, as well as the Doppler power spectrum distributions (PSDs). Numerous simulation results of the propagation characteristic for different physical properties of the tunnel, as well as the different motion properties of the transmitter and receiver, are studied and discussed; they demonstrate that the proposed channel model is suitable for describing the practical V2V tunnel communication scenarios.

Keywords: MIMO channel modeling; space CCFs; temporal ACFs; frequency CCfs; Doppler PSDs

Citation: Zhou, J.; Wu, S.; Lv, Z.; Luo, H.; Liu, T.; Shao, G. Research on Vehicle-to-Vehicle MIMO Wireless Channels in Various Tunnels. *Energies* **2022**, *15*, 5222. https://doi.org/10.3390/en15145222

Academic Editor: Vítor Monteiro

Received: 18 June 2022
Accepted: 12 July 2022
Published: 19 July 2022

1. Introduction

1.1. Backgrounds

As a promising technology for sixth generation (6G) wireless communication systems, multiple-input multiple-output (MIMO) equipment has received increasing attention throughout the industry and academia [1,2], which is mainly due to the significant gains by exploiting the multi-path richness of wireless channels [3]. In light of this, it is of vital importance for the researchers to investigate the propagation characteristics of wireless channels in the physical layer [4]. In the existing literature, such as [5,6], authors are inclined to propose effective channel models to characterize the propagation physical in different vehicle-to-vehicle (V2V) communication scenarios. According to the measured data in [7], it has been demonstrated that three-dimensional (3D) channel models, which consider the azimuth and elevation angles of the propagation paths, are obviously more accurate than two-dimensional (2D) channel models in describing the practical wireless communication environments [8]. In light of this theory, the authors proposed a variety of 3D channel models to describe the practical V2V communication scenarios. Specifically, in [9,10], Jiang et al. and Yuan et al., respectively, developed the multiple confocal semi-ellipsoid models and cylinder models in 3D space to describe the scatterer distributions in V2V communication scenarios. It is worth mentioning that V2V channels are obviously different from the typical channel models, which mainly concentrate on their high dynamic properties; therefore, it is crucial to investigate the impact of the motion properties—motion time, direction, and velocity—on the V2V channel characteristics in the time, space, and frequency domains. This in principle plays an important role in the design and evaluation of the V2V communication systems [11,12].

1.2. Prior Works

It is well known that when we investigate the propagation characteristics of V2V channels, it is necessary to consider different communication scenarios between a transmitter and a receiver, such as streets, tunnels, highways, and so on. To achieve this research goal, we are required to model effective channels to describe the scatterer distributions in V2V communication scenarios [13]. Since the traffic infrastructure throughout the world has been rapidly developed in recent years, wireless communication scenarios behave in a more complicated manner than before, especially the tunnel communications [14,15]. It is worth mentioning that channel models used for wireless communication analysis are typically fundamental in terms of facilitating theoretical analyses and making simulations tractable; therefore, it is important to propose 3D models to describe the V2V channels in tunnel scenarios. Meanwhile, multiple-input multiple-output (MIMO)-assisted vehicle-to-vehicle (V2V) communications, which aim to minimize the number of traffic fatalities, injuries, and accidents while fostering the improvement of new applications, ought to become hotspot scenarios in 6G networks [16,17].

To efficiently study the performance of realistic V2V wireless communication systems, and meanwhile compare different 6G communication proposals, it is essential to gain insights into the underlying propagation characteristics in V2V wireless networks [18]. In the existing literature, there have been many research works concerning MIMO V2V channel modeling. To be specific, the authors proposed a geometry-based MIMO V2V scattering channel model in [19], which used the semi-circular model to describe the scatterer distributions in tunnel communication scenarios. In this study, Avazov et al. derived the correlation property functions to investigate the propagation characteristics of the MIMO V2V tunnel channels in different space domains. In [20], He et al. developed a geometry-based statistical channel model for MIMO V2V communications in tunnel scenarios. In this work, the authors assumed that the propagation waves emerging from the transmitter in wireless channels experienced a single interaction before arriving at the receiver. The authors in [5,21] proposed a twin-cluster channel model to depict the scattering environments in V2V tunnel scenarios. In these research works, some underlying V2V propagation characteristics, such as local correlation properties of the propagation links experiencing the line-of-sight (LoS) and non-LoS (NLoS) paths in the time, space, and frequency domains, were derived and discussed in detail. Furthermore, the authors in [22] studied the high dynamic properties of V2V channels in both the time and frequency domains, which derived the channel impulse response (CIR) to characterize the high dynamic physical properties of the V2V channel model. The authors in [23] proposed a cluster-based non-stationary MIMO channel model to investigate the time variation of the wireless channels in different motion environments by considering the small-scale time-varying parameters, such as the angle of departure (AoD), the angle of arrival (AoA), and the propagation path lengths. In [24], the authors developed a non-wide-sense stationary channel model for MIMO communications in high dynamic vehicular communication systems, which derived the real-time model parameters, i.e., angular parameters and distances from the transmitter/receiver to the cluster, to investigate the non-stationary properties of the channel models. It is worth mentioning that the interfering objects in the aforementioned channel models, which mainly mimic moving vehicles, buildings, and other features, are generally randomly situated in complicated V2V communication environments, such as tunnel scenarios. However, in principle, it is difficult, almost impossible, to determine the position of interfering objects in the propagation characteristics of the V2V channels in the time, space, and frequency domains, which makes it difficult to accurately evaluate the performance of the V2V tunnel communication systems.

1.3. Main Contributions

To solve the aforementioned research problems, we propose a geometry-based channel model for describing the V2V communications in practical tunnel scenarios, as shown in Figure 1. It is worth mentioning that the proposed channel model is for sub 6 GHz, which

is mainly for V2V communications [25,26]. The contributions of this article are summarized as follows:

- We propose a 3D geometry-based stochastic scattering channel model for V2V communications in tunnel scenarios. The impacts of the typical physical properties of the propagation scenarios on the V2V channel characteristics in the time, space, and frequency domains are derived and investigated. The simulation results show that the proposed channel model has the ability to describe the practical V2V communication scenarios.
- In the proposed channel model, the time-varying parameters of the propagation paths and angles are derived to characterize the channel non-stationarity in the time domain. Furthermore, we consider the impacts of the road sections and moving time/directions/speeds of the transmitter and receiver on the correlation properties of different propagation links.
- We derive the correlation property functions of the proposed V2V channel model in the time, space, and frequency domains, which are, respectively, the space cross-correlation functions (CCFs), temporal auto-correlation functions (ACFs), frequency CCFs, as well as the Doppler power spectrum distributions (PSDs). Furthermore, we provide the numerous simulation results of the propagation characteristic for different physical properties of the tunnel, as well as the different motion properties of the transmitter and receiver.
- The proposed algorithm for V2V channel modeling considers the balance between generality and complexity. To be specific, when we properly adjust the model parameters, such as the Rician factor and motion time/velocities/directions of the transmitter and receiver, the proposed channel model has the ability to characterize the main propagation characteristics for V2V communications in tunnel scenarios, which shows the generality of the proposed V2V channel model.

The rest of this paper is organized as follows: In Section 2, we describe the system channel model for V2V communications in tunnel scenarios. In Section 3, the physical properties of the proposed propagation channel model for V2V tunnel communication scenarios are discussed. In Section 4, we derive the correlation property functions of the proposed V2V channel model in the time, space, and frequency domains, such as the space CCFs, temporal ACFs, frequency CCFs, as well as the Doppler PSDs. In Section 5, we give the simulation and theoretical results of the propagation characteristics of the proposed V2V channel model for tunnel scenarios. Finally, a summary and outlook are given in Section 6.

(**a**) (**b**)

Figure 1. Various geometrical tunnels. (**a**) Rectangular tunnel. (**b**) Rectangular tunnel without ceiling.

2. Geometrical Tunnel Propagation Model

It is worth mentioning that the transmitter and receiver are equipped with low elevation antennas in V2V channel model for tunnel communication scenarios, as shown in Figure 1. The V2V channel models in the prior works are mainly for open communication environments, which are not suitable for characterizing the high dynamic propagation

properties of the V2V channel models, especially the tunnel communication scenarios. Furthermore, we notice that the structures of the tunnels are complicated and changeable, which bring us difficulty in building a general channel model to effectively describe the V2V communications in tunnel scenarios. To solve this issue, we conducted the research in this paper. In many studies in the literature, the diffuse, LoS, and SPE scattering components occupy the vast majority of the whole. Hence, the components all need to be considered. Otherwise, since different channel characteristics are for different geometries, they can describe the propagation as rectangle-like or ellipse-like tunnels. Here, the channel model describes the scattering environments inter-tunnel with a length of L. It is assumed that the cross section is semi-oval with radius R_a and R_b, shown in Figure 2; the rectangular or semi-rectangular tunnels with width $W = 2R_a$ and height $H = R_b$, respectively, are shown in Figure 3.

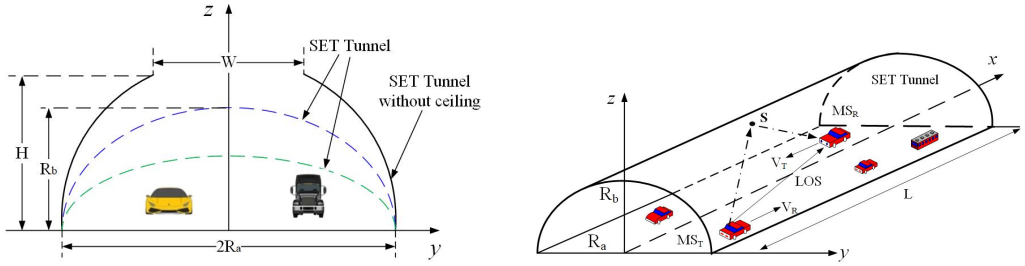

(**a**) (**b**)

Figure 2. Propagation scenario in SET and SET without ceiling. (**a**) SET. (**b**) SET without ceiling.

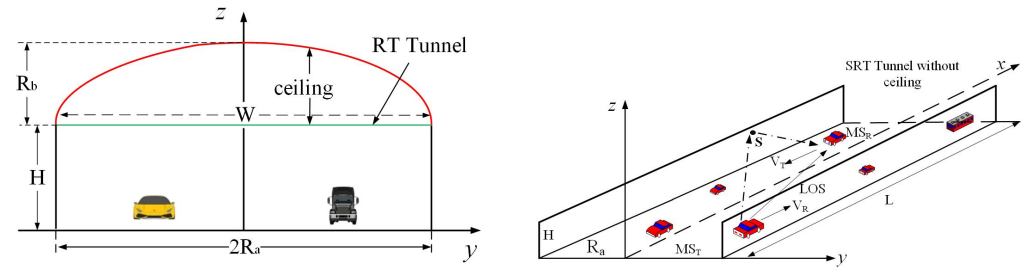

(**a**) (**b**)

Figure 3. Propagation scenarios in RT and in SRT with an arch ceiling. (**a**) RT. (**b**) RT without ceiling.

It is assumed that the scatters are randomly distributed on the tunnel inter-surfaces, as shown in Figure 4, where the coordinates of the reference scatter are expressed as $m = 1, 2, \ldots, +\infty$, $n = 1, 2, \ldots, +\infty$, and $o = 1, 2, \ldots, +\infty$. For similarity, we define $z = R_b\sqrt{1-(y/R_a)^2}$ for SET, $z = \sqrt{R^2 - y^2}$ for SET and $0 \leq z \leq R_b$ for SRT. This allows us to present the position of the reference scatter $S^{(m,n,o)}$ by (x_m, y_n, z_o), where x_m and y_n are random variables. Hence, the distribution of the scatters is completely determined by the distribution of x_m and y_n. Figure 4 shows MS_T and MS_R, the mean the vehicle transmitter and receiver, respectively. We assumed that the transceivers carry a uniform linear MIMO array, consisting of M_T and M_R antenna elements. Spacing of antenna units is indicated by δ_T and δ_R, respectively. The moving direction of the transceivers in the xy-plane relative to the x-axis are denoted by the angles γ_T and γ_R. Similarly, the elevation angles of the transceivers with respect to the xy-plane are described by φ_T and φ_R, respectively. The coordinates of the MIMO arrays of MS_T and MS_R are indicated by (x_T, y_T, z_T) and (x_R, y_R, z_R). It is also supposed that MS_T and MS_R are inside the tunnels, such that $0 \leq x_T \leq x_R \leq L$ and $-R_a \leq y_T \leq y_R \leq R_a$ for SET. This is considering the LoS component between MS_T and MS_R. Similarly, $\alpha_T^{(m,n,o)}$, $\alpha_R^{(m,n,o)}$, $\beta_T^{(m,n,o)}$ and $\beta_R^{(m,n,o)}$ indicate AAOD, AAOA, EAOD, and EAOA angles, respectively. The transceivers move at a speed of v_T and v_R in an angle of ϕ_v^T and ϕ_v^R with respect to the x-axis. $D_T^{(m,n,o)}$ represents the

path distance between A_T^l and $S^{(m,n,o)}$; $D_R^{(m,n,o)}$ represents the path distances of $S^{(m,n,o)}$ to A_R^k. The path of A_T^l through $S^{(m,n,o)}$ to A_R^k is NLoS propagation, and $D_{LoS}^{(m,n,o)}$ represents the LoS path distance of A_T^l to A_R^k.

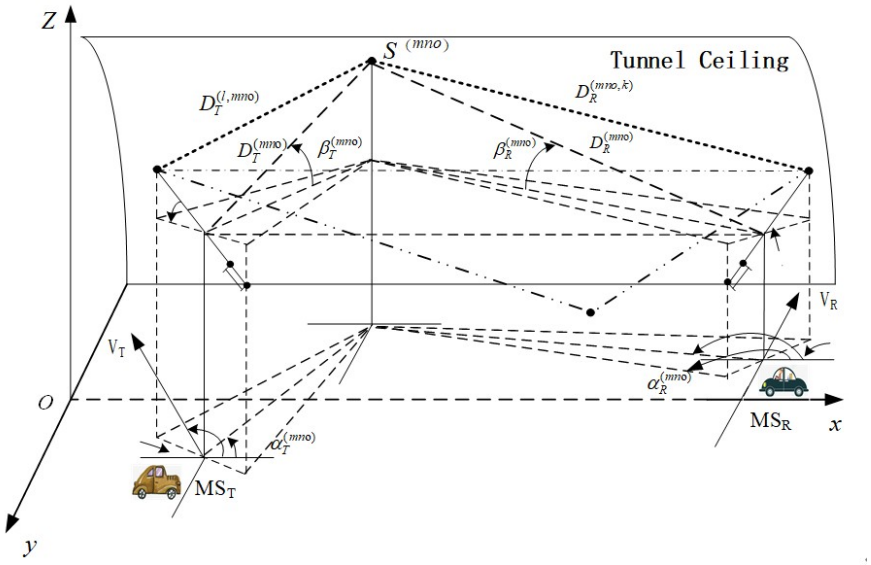

Figure 4. Geometrical scattering model for SET.

In order to simulate the V2V communication for tunnel scenarios, we mainly make the following assumptions: (1) The scatters distribute on the tunnel inter-surfaces, and the number of scatters approaches infinity, that is $M, N, O \to +\infty$, ignoring the interference of other scatterers in or out of the tunnel, which can be considered as the omnidirectional radiation element, and both have the same reflection coefficient, so it will not cause reflection LoSs. (2) Transceivers M_T and M_R are in the same horizontal plane, and only the influence of scatters from the transceiver is considered. According to the geometric relationships in Figures 2–4, the angular parameters of the propagation links in the azimuth and elevation planes can be, respectively, expressed as

$$\alpha_i(x_m, y_n) = \begin{cases} f(x_m, y_n), & y_n \geq y_i \\ -f(x_m, y_n), & y_n \leq y_i \end{cases}, \tag{1}$$

$$\beta_i(x_m, y_n, z_o) = \begin{cases} -g(x_m, y_n, z_o), & z_o \geq z_i \\ g(x_m, y_n, z_o), & z_o \leq z_i \end{cases}, \tag{2}$$

where

$$f(x_m, y_n) = \arccos \frac{x_m - x_i}{\sqrt{(x_m - x_i)^2 + (y_n - y_i)^2}}, \tag{3}$$

$$g(x_m, y_n, z_o) = \arccos \frac{\sqrt{(x_m - x_i)^2 + (y_n - y_i)^2}}{\sqrt{(x_m - x_i)^2 + (y_n - y_i)^2 + (z_o - z_i)^2}}, \tag{4}$$

where $i = T$ and $i = R$ stand for the transmitter and receiver, respectively. It is assumed that the number of the scatterers in the proposed V2V channel model is infinite, which means $M, N, O \to +\infty$. The parameters x_m, y_n, and z_o can be represented by the successive random variables x, y, and z, respectively. Furthermore, we assume that the effective

scatters are uniformly distributed on the tunnel inter-surface in the proposed V2V channel model; therefore, we have

$$P_x(x) = \frac{1}{x_R - x_T}, \quad x \in [x_T, x_R], \tag{5}$$

$$P_y(y) = \frac{1}{W}, \quad y \in [-\frac{W}{2}, \frac{W}{2}]. \tag{6}$$

It can be observed from the geometric channel model that the expression of z can be derived by $z = (W \tan \alpha)/2$, where α is evenly distributed within $[0, \arctan(2H/W)]$. Therefore, the PDF can be expressed as

$$P_z(z) = \frac{2W}{(W^2 + 4z^2) \arctan \frac{2H}{W}}, \quad z \in [0, H]. \tag{7}$$

Based on the expressions of the PDFs of x, y and z, the joint PDF $P_{xyz}(x, y, z)$ can be expressed as

$$P_{xyz}(x, y, z) = \frac{2}{(x_R - x_T)(W^2 + 4z^2) \arctan(2H/W)}, \\ x \in [x_T, x_R], y \in [-\frac{W}{2}, \frac{W}{2}], z \in [0, H]. \tag{8}$$

Furthermore, the joint PDF $P_{xy}(x, y)$ can be expressed as

$$P_{xy}(x, y) = \frac{1}{W(x_R - x_T)}, \quad x \in [x_T, x_R], y \in [-\frac{W}{2}, \frac{W}{2}]. \tag{9}$$

3. Channel Analysis for V2V MIMO in Tunnels

3.1. V2V MIMO Channel Model

In the proposed V2V channel model, we define the reference scatter on the tunnel inter-surfaces as $S^{(m,n,o)}$, where the variables m, n and o are infinite in the 3D coordinate system. Then the V2V MIMO channel can be described by an $M_R \times M_T$ channel matrix, $H_{kl}(\tau', t) = [h_{kl}(\tau', t)]_{M_R \times M_T}$, where $h_{kl}(\tau', t)$ presents the time-variant impulse response. The TVTF indicated by $H_{kl}(f', t)$ can be simply analyzed, and is the Fourier transform of $h_{kl}(\tau', t)$; then the $H_{kl}(f', t)$ of the reference model can be expressed as [27,28]

$$H_{kl}(f', t) = H_{kl}^{Dif}(f', t) + H_{kl}^{LoS}(f', t) + H_{kl}^{Spe}(f', t), \tag{10}$$

where $H_{kl}^{Dif}(f', t)$, $H_{kl}^{LoS}(f', t)$, and $H_{kl}^{Spe}(f', t)$ are assumed to be independent, and stand for the impulse responses of the diffuse, LoS, and specular propagation components, respectively. Based on the assumptions that only considering single-bounce scattering components, the scattered signal from the transmitter from the MIMO l-th transmitter antenna unit $A_T(l)$ travels over the scatter $S^{(m,n,o)}$ before being received at the MIMO l-th receiver antenna unit $A_R(k)$, shown in Figure 4, then $H_{kl}^{Dif}(f', t)$ in Equation (10) from MIMO antenna element $A_T(l)$ to $A_R(k)$ can be expressed as

$$H_{kl}^{Dif}(f', t) = \lim_{\substack{M \to \infty \\ N \to \infty \\ O \to \infty}} \frac{1}{\sqrt{(c_R + 1)MNO}} \sum_{m,n,o=1}^{M,N,O} \\ \times e^{-j\frac{2\pi}{\lambda} D_{kl}^{(mno)} + j[2\pi(f_T^{(mno)} + f_R^{(mno)})t + \theta^{(mno)} - 2\pi\tau_{kl}^{(mno)} f']}, \tag{11}$$

where

$$D_{kl}^{(mno)} = D_{T}^{(l,mno)} + D_{R}^{(mno,k)}, \tag{12}$$

$$\begin{aligned} D_{T}^{(l,mno)} &= \sqrt{(x_m - x_T)^2 + (y_n - y_T)^2 + (z_o - z_T)^2} \\ &- (M_T - 2l + 1) \\ &\times \frac{\delta_T}{2}\left[\cos\phi_T \cos\beta_T^{(mno)} \cos(\gamma_T - \alpha_T^{(mno)}) + \sin\phi_T \sin\beta_T^{(mno)} \right], \end{aligned} \tag{13}$$

$$\begin{aligned} D_{R}^{(mno,k)} &= \sqrt{(x_m - x_R)^2 + (y_n - y_R)^2 + (z_o - z_R)^2} \\ &- (M_R - 2k + 1) \\ &\times \frac{\delta_R}{2}\left[\cos\phi_R \cos\beta_R^{(mno)} \cos(\gamma_R - \alpha_R^{(mno)}) + \sin\phi_R \sin\beta_R^{(mno)} \right], \end{aligned} \tag{14}$$

$$f_T^{(mno)} = f_{T_{max}} \cos(\alpha_T^{(mno)} - \varphi_v^T) \cos\beta_T^{mno}, \tag{15}$$

$$f_R^{(mno)} = f_{R_{max}} \cos(\alpha_R^{(mno)} - \varphi_v^R) \cos\beta_R^{mno}. \tag{16}$$

In Equation (11), the phase $\theta^{(mno)}$ is related to the plane wave and the scatter, which is assumed to be independently randomly distributed in the interval $[\,0, 2\pi\,)$. The $\tau_{kl}^{(mno)}$ stands for the propagation delay of the diffuse reflection components, which can be derived by $\tau_{kl}^{(mno)} = D_{kl}^{(mno)}/c_o$, where c_o is the speed of light. In Equations (15) and (16), $f_{T_{max}}$ and $f_{R_{max}}$ represent the maximum Doppler associated with the transmitter and receiver, which can be, respectively, calculated by $f_{T_{max}} = v_T/\lambda$ and $f_{R_{max}} = v_R/\lambda$, with λ representing the wavelength. For the LoS propagation links, the complex channel response can be written by

$$H_{kl}^{LoS}(f', t) = \sqrt{\frac{c_R^{LoS}}{c_R + 1}} e^{-j\frac{2\pi}{\lambda} D_{LoS}^{(l,k)} + j2\pi\left[(f_T^{(0)} + f_R^{(0)})t - \tau_{kl}^{(0)} f' \right]}, \tag{17}$$

where

$$\begin{aligned} D_{LoS}^{(l,k)} &= \sqrt{(x_R - x_T)^2 + (y_R - y_T)^2 + (z_R - z_T)^2} \\ &- (M_T - 2l + 1)\frac{\delta_T}{2}\cos\phi_T \cos\gamma_T - (M_R - 2k + 1)\frac{\delta_R}{2}\cos\phi_R \cos\gamma_R, \end{aligned} \tag{18}$$

$$f_T^{(0)} = f_{T_{max}} \cos(\alpha_T^{(0)} - \varphi_v^T) \cos\beta_T^0, \tag{19}$$

$$f_R^{(0)} = f_{R_{max}} \cos(\alpha_R^{(0)} - \varphi_v^R) \cos\beta_R^{(0)}, \tag{20}$$

where $\alpha_T^{(0)}$, $\beta_T^{(0)}$, $\alpha_R^{(0)}$, and $\beta_R^{(0)}$, respectively, stand for the AAOD, EAOD, AAOA, and EAOD of the NLoS propagation links in the proposed V2V channel model. Furthermore, the specular component $H_{kl}^{Spe}(f', t)$ in the TVTF Equation (10) can be expressed as

$$H_{kl}^{Spe}(f', t) = \sqrt{\frac{c_R^{Spe}}{c_R + 1}} e^{-j\frac{2\pi}{\lambda} D_{Spe}^{(l,k)} + j2\pi\left[(f_T^{(1)} + f_R^{(1)})t - \tau_{kl}^{(1)} f' \right]}, \tag{21}$$

where

$$D_{Spe}^{(l,k)} = \sqrt{(x_s - x_T)^2 + (y_s - y_T)^2 + (z_s - z_T)^2} + \sqrt{(x_s - x_R)^2 + (y_s - y_R)^2 + (z_s - z_R)^2}, \quad (22)$$

$$f_T^{(1)} = f_{T_{max}} \cos(\alpha_T^{(1)} - \varphi_v^T) \cos\beta_T^1, \quad (23)$$

$$f_R^{(1)} = f_{R_{max}} \cos(\alpha_R^{(1)} - \varphi_v^R) \cos\beta_R^{(1)}, \quad (24)$$

where $\alpha_T^{(1)}$, $\beta_T^{(1)}$, $\alpha_R^{(1)}$, and $\beta_R^{(1)}$, respectively, represent AAOD, EAOD, AAOA, and EAOA of the specular propagation links. In Equations (11), (17), and (21), the symbol c_R represents the summation of the Rice factors c_R^{LoS} and c_R^{Spe}, which can be derived by the ratio of the average power of the LoS and specular components with respect to the diffuse component, i.e., $c_R^{LoS} = E\{|H_{kl}^{LoS}(f',t)|^2\}/E\{|H_{kl}^{Dif}(f',t)|^2\}$ and $c_R^{Spe} = E\{|H_{kl}^{Spe}(f',t)|^2\}/E\{|H_{kl}^{Dif}(f',t)|^2\}$. Similar to the above analysis for SET, the TVTF of SCT can be derived similarly to Equation (11); we have

$$H_{kl}^{Dif}(f',t) = \lim_{\substack{M\to\infty \\ N\to\infty}} \frac{1}{\sqrt{(c_R+1)MN}} \sum_{m,n=1}^{M,N} \times e^{-j\frac{2\pi}{\lambda}D_{kl}^{(m,n)} + j\left[2\pi(f_T^{(m,n)} + f_R^{(m,n)})t + \theta^{(m,n)} - 2\pi\tau_{kl}^{(m,n)}f'\right]}, \quad (25)$$

$$H_{kl}^{LoS}(f',t) = \sqrt{\frac{c_R^{LoS}}{c_R+1}} e^{-j\frac{2\pi}{\lambda}D_{LoS}^{(l,k)} + j2\pi\left[f^{(0)}t - \tau_{kl}^{(0)}f'\right]}, \quad (26)$$

$$H_{kl}^{Spe}(f',t) = \sqrt{\frac{c_R^{Spe}}{c_R+1}} e^{-j\frac{2\pi}{\lambda}D_{Spe}^{(l,k)} + j2\pi\left[f^{(1)}t - \tau_{kl}^{(1)}f'\right]}. \quad (27)$$

Differently from derivations for SET and SCT above, TVTF indicated by $H_{kl}(f',t)$ of SRT can be expressed as

$$H_{kl}(f',t) = H_{kl}^{Dif}(f',t) + H_{kl}^{LoS}(f',t). \quad (28)$$

3.2. Cross Correlation Functions of V2V MIMO Channel

It is well known that the propagation links in V2V wireless channels have different correlation properties in different time, space, and frequency domains. In the existing literature, the authors are inclined to adopt the space-time-frequency cross-correlation functions (STF CCFs) to study the correlation properties of propagation links in the V2V channels in the time, space, and frequency domains. In light of this, we follow this research solution in the following parts. In the proposed channel model, the CCF between the TVTF $H_{kl}(f',t)$ and $H_{k'l'}(f',t')$ for MIMO antenna arrays can be expressed as [29]

$$\rho_{kl,k'l'}(\delta_T,\delta_R,v',\tau) = E\{H_{kl}^*(f',t)\cdot H_{k'l'}^*(f'+v',t+\tau)\} \times \rho_{kl,k'l'}^{Dif}(\delta_T,\delta_R,v',\tau) + \rho_{kl,k'l'}^{LoS}(\delta_T,\delta_R,v',\tau) + \rho_{kl,k'l'}^{Spe}(\delta_T,\delta_R,v',\tau), \quad (29)$$

where * denotes the complex conjugate, and the statistical expectation operator $E\{\cdot\}$ means the expectation operator of all random variables. By using Equations (11), (17), and (21), the space-time-frequency CCF $\rho_{kl,k'l'}(\delta_T, \delta_R, v', \tau)$ of the diffuse, LoS, and specular propagation components can be expressed as

$$\rho^{Dif}_{kl,k'l'}(\delta_T, \delta_R, v', \tau) = \lim_{\substack{M\to\infty \\ N\to\infty \\ O\to\infty}} \frac{1}{\sqrt{(c_R+1)MNO}} \sum_{m,n,o=1}^{M,N,O} E\{c^{(mno)}_{ll'} \cdot d^{(mno)}_{kk'} \times e^{j2\pi\left[(f^{(mno)}_T + f^{(mno)}_R)\tau - \tau\prime^{(mno)}_{kl} v\prime\right]}\}, \quad (30)$$

where

$$c^{(mno)}_{ll'} = e^{j2\pi\frac{\delta_T}{\lambda}(l-l')\cos\phi_T \cos\beta^{(mno)}_T \cos(\gamma_T - \alpha^{(mno)}_T)} \times e^{j2\pi\frac{\delta_T}{\lambda}(l-l')\sin\phi_T \sin\beta^{(mno)}_T}, \quad (31)$$

$$d^{(mno)}_{kk'} = e^{j2\pi\frac{\delta_R}{\lambda}(k-k')\cos\phi_R \cos\beta^{(mno)}_R \cos(\gamma_R - \alpha^{(mno)}_R)} \times e^{j2\pi\frac{\delta_R}{\lambda}(k-k')\sin\phi_R \sin\beta^{(mno)}_R}, \quad (32)$$

The above expressions are obtained by averaging the random phase $\theta^{(mno)}$. Therefore, the CCF $\rho^{Dif}_{kl,k'l'}(\delta_T, \delta_R, v', \tau)$ of the diffuse reflection component can be expressed as

$$\rho^{Dif}_{kl,k'l'}(\delta_T, \delta_R, v', \tau) = \frac{2}{(x_R - X_T)\arctan\frac{2H}{W}(C_R+1)} \times \int_0^H \int_{-W/2}^{W/2} \int_{x_T}^{X_R} d_{kk'}(x,y,z) c_{ll'}(x,y,z) \times e^{j2\pi[(f_T(x,y,z)+f_R(x,y,z))\tau - \tau\prime^{(x,y,z)}_{kl} v\prime]} \times \frac{1}{(W^2+4z^2)} dx dy dz, \quad (33)$$

where

$$c_{ll'}(x,y,z) = e^{j2\pi\frac{\delta_T}{\lambda}(l-l')\cos\phi_T \cos\beta_T(x,y,z)\cos(\gamma_T - \alpha_T(x,y,z))} \times e^{j2\pi\frac{\delta_T}{\lambda}(l-l')\sin\phi_T \sin\beta_T(x,y,z)} \quad (34)$$

$$d_{kk'}(x,y,z) = e^{j2\pi\frac{\delta_R}{\lambda}(l-l')\cos\phi_R \cos\beta_R(x,y,z)\cos(\gamma_R - \alpha_R(x,y,z))} \times e^{j2\pi\frac{\delta_R}{\lambda}(l-l')\sin\phi_R \sin\beta_R(x,y,z)}, \quad (35)$$

$$f_T(x,y,z) = f_{T_{max}} \cos(\alpha_T(x,y,z) - \varphi^T_v)\cos\beta_T(x,y,z), \quad (36)$$

$$f_R(x,y,z) = f_{R_{max}} \cos(\alpha_R(x,y,z) - \varphi^R_v)\cos\beta_R(x,y,z), \quad (37)$$

$$\tau\prime^{(x,y,z)}_{kl} = \frac{1}{c_o}\left(D^{(l)}_T(x,y,z) + D^{(k)}_R(x,y,z)\right), \quad (38)$$

where $\alpha_T(x,y,z)$, $\alpha_R(x,y,z)$, $\beta_T(x,y,z)$, and $\beta_R(x,y,z)$ denote the coordinate of the scatterers in the x-, y-, and z-axes, respectively. According to Equation (38), $\tau\prime^{(x,y,z)}_{kl}$ can be

calculated from $D_T^{(l)}(x,y,z)$ and $D_R^{(k)}(x,y,z)$. By using Equations (13) and (14), the distances $D_T^{(l)}(x,y,z)$ and $D_R^{(k)}(x,y,z)$ can be expressed as

$$D_T^{(l)}(x,y,z) = D_T(x,y,z) - (M_T - 2l + 1)\frac{\delta_T}{2} \times \left[\cos\phi_T \cos\beta_T(x,y,z) \cos\left(\gamma_T - \alpha_T(x,y,z)\right) + \sin\phi_T \sin\beta_T(x,y,z) \right], \quad (39)$$

$$D_R^{(k)}(x,y,z) = D_R(x,y,z) - (M_R - 2k + 1)\frac{\delta_R}{2} \times \left[\cos\phi_R \cos\beta_R(x,y,z) \cos\left(\gamma_R - \alpha_R(x,y,z)\right) + \sin\phi_R \sin\beta_R(x,y,z) \right], \quad (40)$$

where $D_T(x,y,z)$ and $D_R(x,y,z)$ account for the distances from the scatter coordinate (x,y,z) to the vehicle transceivers, respectively. Referring to the derivations of TVTF of SET, it is not difficult to derive the model of SCT and SRT. The CCF of tunnels can be obtained by

$$\rho_{kl,k'l'}^{Dif}(\delta_T,\delta_R,v',\tau) = \frac{1}{2R(x_R - x_T)(c_R + 1)} \times \int_{-R}^{R}\int_{x_T}^{X_R} d_{kk'}(x,y)c_{ll'}(x,y) \times e^{j2\pi\left[f(x,y)\tau - \tau'^{(x,y)}_{kl} v'\right]} dxdy. \quad (41)$$

Based on the aforementioned derivations of the space CCFs, temporal ACFs, frequency CCFs, and Doppler PSDs, we are able to investigate the propagation characteristics of the proposed V2V channel model for tunnel scenarios in the time, space, and frequency domains. This provides us with diversified perspectives for investigating the physical properties of the LoS and NLoS propagation links. In the following section, we will investigate the correlation properties of the propagation links with respect to the Rician factor, the motion properties of the transmitter and receiver.

4. Channel Capacity and Doppler of V2V MIMO

To improve the performances of wireless communications, the improvement of the spectral efficiency or the reduction of the bit error rate is obviously emphasized, so the path between the antenna elements of the transmitter and the receiver has a great influence on the transmission performance. While a large number of diffuse and specular components are distributed in the tunnel environment, one needs to know whether the number of active modes will bring enough spatial correlation and distribution of the singular values of the channel H matrix to significantly reduce the capacity and Doppler of V2V communication. The capacity can be used to fully characterize the MIMO, which is of great significance for designing the system. Past studies in the literature have addressed the Independent Identical Distribution (IID) complex Gauss channel model, which has laid the theoretical foundation for channel capacity. Here, we will use spatial CCF $\rho_{kl,k'l'}(\delta_T,\delta_R)$ to explore their important impacts on the MIMO system and describe the statistical characteristics by complementary cumulative distribution function and Ergodic capacity. Usually, if the exact channel characteristics are not known to the system, the optimal method is to distribute the power equally to each antenna element, and the average channel capacity can be expressed as

$$\begin{aligned} \bar{C} &= E[\log 2det(I_{N_r} + \frac{SNR}{N_t} H \cdot H^T)] \\ &= E[\log 2det(I_{N_r} + \frac{P}{N_t\sigma^2} R_r^{1/2} H_W R_t H_W^T (R_r^T)^{1/2})]. \end{aligned} \quad (42)$$

In Equation (42), N_r and N_t are the number of antenna elements at the receiving and transmitting stations, respectively. In the case of IID, channel matrix H can be expressed as

$H = R_r^{1/2} H_W (R_t^{1/2})^T$, where R_r and R_t denote the $N_r \times N_r$ and $N_t \times N_t$ correlation matrixes of the receiving and transmitting antenna arrays. Generally H_W is the independent and identically distributed $R_r \times R_t$ complex Gauss random matrix and I_{N_r} is the unit matrix. When the noise is Gaussian, the signal-to-noise ratio of the channel can be expressed as SNR. The robustness of MIMO in terms of coping with the high correlation among the antenna elements, strongly depends on the antenna array architecture. Here, use Maximum Ratio Combining (MRC) to measure the different response of the power spectrum and the standard deviation in the Binary-Phase-Shift-Keying (BPSK) modulation. Therefore, the BER of the multi-antenna arrays can be computed as

$$P_e = \frac{1}{2} \sum_{k=1}^{K} \pi_k (1 - \sqrt{\frac{\lambda_k}{\lambda_k + 1}}), \tag{43}$$

where $\pi_k = \prod_{i=1}^{N} (\frac{\lambda_k}{\lambda_k - \lambda_i}), i \neq k$. In Equation (43), λ_k is the k-th eigenvalue of spatial CCF matrix R_r. So far, we can obtain the required eigenvalues by decomposition of the spatial CCF matrix, where the matrix elements have been derived in the previous sections. The eigenvalue decomposition formula can be expressed as

$$R_r = U \beta V^H, \tag{44}$$

where the matrices U and V denote the unit matrix and β is the diagonal matrix. We have

$$R_r = \begin{bmatrix} 1 & \rho_{k'l^{prime}}(\delta_R) \\ \rho_{k'l^{prime}}(\delta_T) & 1 \end{bmatrix} \tag{45}$$

where R_r is the SFC matrix for a two-element MIMO array, the eigenvalues can be solved directly and simply from $|\lambda E - R_r| = 0$, which can be derived by

$$\lambda_{1,2} = 1 \pm \sqrt{\rho_{k'l'}(\delta_T) \times \rho_{k'l'}(\delta_R)}. \tag{46}$$

Then, the CDF $F(\gamma \leq x)$ of the output SNR γ can be analyzed and studied when the eigenvalues of the spatial CCF matrix are expressed as

$$F(\gamma \leq x) = \frac{1}{\lambda_1 - \lambda_2} [\lambda_1 (1 - e^{x/\lambda_1}) - \lambda_2 (1 - e^{x/\lambda_2})]. \tag{47}$$

It is well known that the Fourier change of the temporal ACF $\rho_{kl}(\tau)$ can obtain the Doppler Power Spectral Density (DPSD), $S_f(f) = F_\tau\{\gamma_{kl}(\tau)\}$. Hence, the DPSD can be expressed as

$$S_f(f) = F_\tau\{\gamma_{kl}(\tau)\} = \int_{-\infty}^{+\infty} \gamma_{kl}(\tau) e^{-j2\pi f \tau} d\tau. \tag{48}$$

From Equation (48), two important metrics to measure DPSD $S_f(f)$, i.e., the average Doppler shift f_{shift} and the Doppler spread f_{spread} are defined as the first moment of $S_f(f)$ and the square root of the second central moment of $S_f(f)$, respectively. f_{shift} and f_{spread} can be computed alternately by using Fourier transform techniques. Therefore, we have

$$f_{shift} = \frac{1}{2\pi j \cdot \rho_{kl}(\tau)} \cdot \frac{\partial \rho_{kl}(\tau)}{\partial \tau}|_{\tau=0} \tag{49}$$

$$f_{spread} = \frac{1}{2\pi} \sqrt{\frac{1}{\rho_{kl}^2(\tau)} \cdot (\frac{\partial \rho_{kl}(\tau)}{\partial \tau})^2 - \frac{1}{\rho_{kl}(\tau)} \cdot \frac{\partial^2 \rho_{kl}(\tau)}{\partial^2 \tau}|_{\tau=0}}. \tag{50}$$

5. Numerical Results and Discussions

In this section, we will investigate the correlation properties of the propagation links in the proposed V2V channel model for tunnel scenarios. The space CCFs, temporal ACFs, frequency CCFs, as well as the Doppler PSDs are studied with respect to the different model parameters. Here, we consider the tunnels with a length of $L = 100$ m and a width 10 m. With reference to Figures 2–4, the length of the long axis and the short axis of the elliptical tunnel are 10 m and 8 m, respectively. In the Figure 3, the side length of the rectangular tunnel is 10 m. The locations of the V2V transmitter and the receiver are defined by the Cartesian coordinates $(x_T, y_T, z_T) = (20, 2, 1)$ and $(x_R, y_R, z_R) = (40, 20, 1)$. Other data parameters are set as follows $\varphi_v^T = \varphi_v^R = 0$, $\gamma_T = \gamma_R = 45^\circ$, $\phi_T = \phi_R = 45^\circ$, and $f_{T_{max}} = f_{R_{max}} = 91$ Hz.

5.1. Channel Characteristics of SET with and without Ceilings

Figure 5 shows the effects of the cross-sectional size of the semi-elliptical on the correlation properties. It can be seen that when we increase the values of the antenna element spacings δ_T and δ_R from 0 to 3, the space correlations of the proposed channel model gradually decrease from 1 to 0, in agreements with the results in [30], verifying the correctness of the simulations and derivations in (33). Furthermore, we notice that when the distances between antenna elements are $\delta_T = \delta_R = 0$, the spatial CCFs of SET reaches the maximum value 1. However, the absolute value of the SET without ceiling is 0.37. Compared with Figure 5 in the LoS scenario, the Rice distribution factor is $c_R = 1$, the SCCF is given in Figure 6 for a LoS propagation scenario. As in Figure 6, the TVTF $H(f, t)$ and $H(f + v, t + \tau)$ are highly correlated; the same results are shown even for relatively large spacing between the antenna elements.

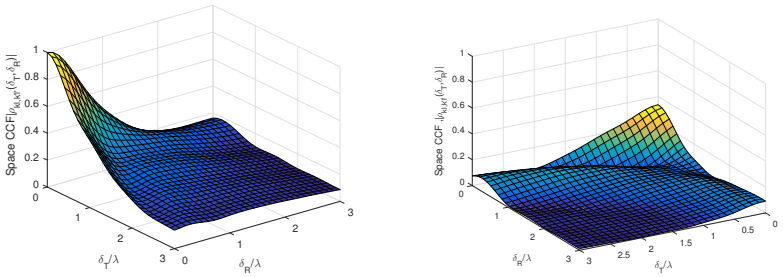

(**a**) (**b**)

Figure 5. Spatial cross-correlation functions of SET and without ceiling for NLoS scenario $(c_R = 0)$. (**a**) SCCF of SET. (**b**) SCCF of SET without ceiling.

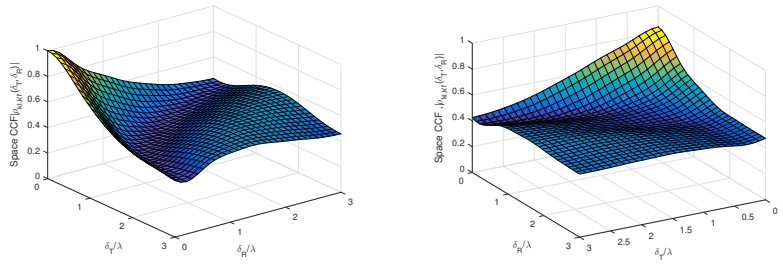

(**a**) (**b**)

Figure 6. Spatial cross-correlation functions of SET and without ceiling for LoS scenario $(c_R = 1)$. (**a**) SCCF of SET. (**b**) SCCF of SET without ceiling.

It is worth mentioning that when the transmitter and receiver move in the same direction in V2V channels, the temporal ACFs of the proposed channel model for different Rice factors c_R are as shown in Figure 7a. It can be observed that when we increase the

motion time, the temporal correlations of the proposed channel model gradually decrease from 1 to 0, and are in agreement with the results in [11,12], verifying the correctness of the simulations and derivations. It can also be seen that when we set τ as zero, the temporal ACFs of normal SET is 1, while the others are one below 1, as shown in Figure 7b, which demonstrates that SET without ceilings fluctuates more obviously. Figure 8 shows the frequency CCFs of the proposed channel model in different communication situations. It can be seen that there is almost no serious fluctuation as to without ceiling, because of more scatters by the tunnels with the ceiling. Overall, the simulation results in Figures 7 and 8 are consistent with the corresponding analytical results, thereby validating the accuracy of the analysis.

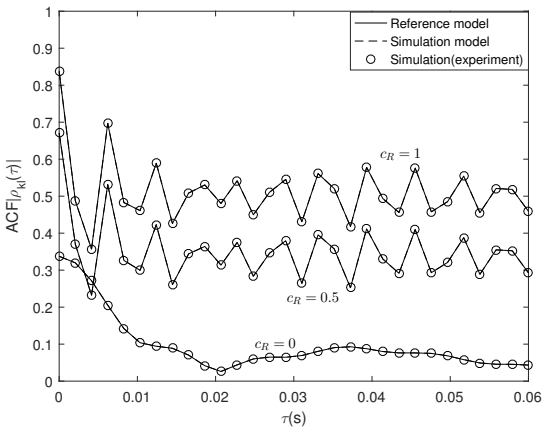

(**a**)

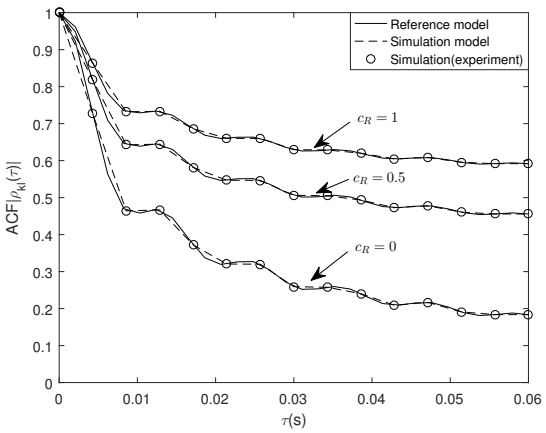

(**b**)

Figure 7. ACF of SET and without ceiling for different Rice factors c_R. (**a**) ACF of SET. (**b**) ACF of SET without ceiling.

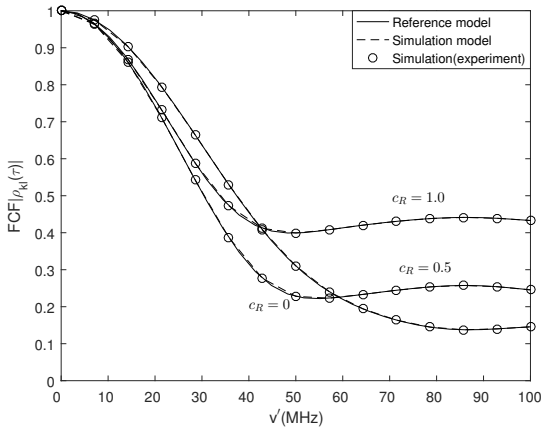

(**a**)

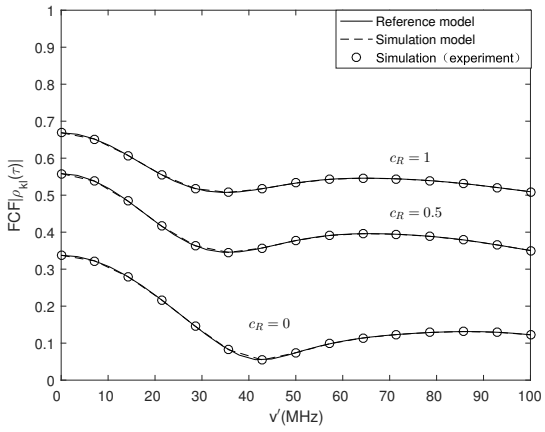

(**b**)

Figure 8. FCF of SET and without ceiling for different Rice factors c_R. (**a**) FCF of SET. (**b**) FCF of SET without ceiling.

Figure 9 shows the frequency CCFs of the proposed V2V channel model for tunnel scenarios with respect to the tunnel size. It is not difficult to see that the resulting values gradually decrease as the scattering range increases. Furthermore, if the cross-sectional area of the tunnel increases, the coherence bandwidth of the proposed channel also decreases. In Figure 9, when the tunnel width R_a is increased from 10 to 16 m, the coherence bandwidth is reduced from 40 to 20 MHz. The coherence bandwidth is more susceptible to frequency fluctuations due to more severe interference from scattering paths in the tunnel. Other verification results are not possible due to the lack of required V2V channel measurement data in other literature studies. However, validating the proposed channel against other channel statistics may be the subject of future research.

Figure 10 depicts the Doppler PSDs of the proposed V2V channel model with respect to the different heights of the tunnel and different relative motion directions of the transmitter and receiver. It can be found that when the transmitter and receiver move in the same directions, the values of the Doppler PSDs behave according to U-shaped distribution. On the other hand, when the transmitter and receiver move in the other directions, the Doppler PSDs decrease gradually. Furthermore, as the tunnel height rises, the value of Doppler PSDs rises as well. Meanwhile, the Doppler PSD value increases as the tunnel height increases.

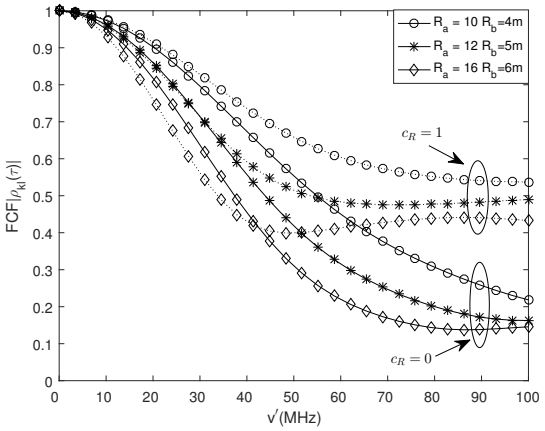

(**a**)

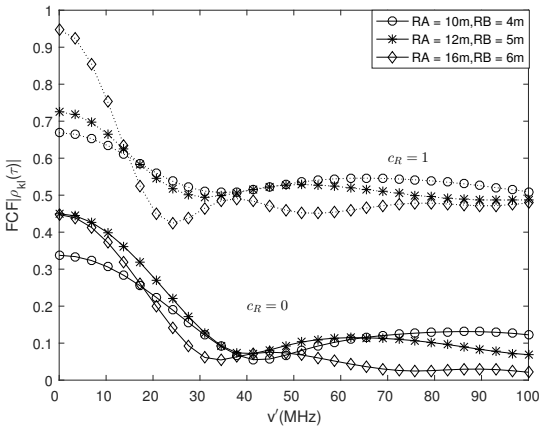

(**b**)

Figure 9. FCF of SET and without ceiling for tunnel parameters for LoS and NLoS. (**a**) FCF of SET. (**b**) FCF of SET without ceiling.

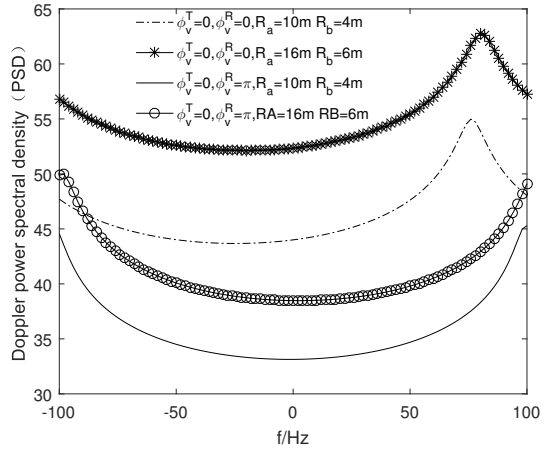

(**a**)

Figure 10. *Cont.*

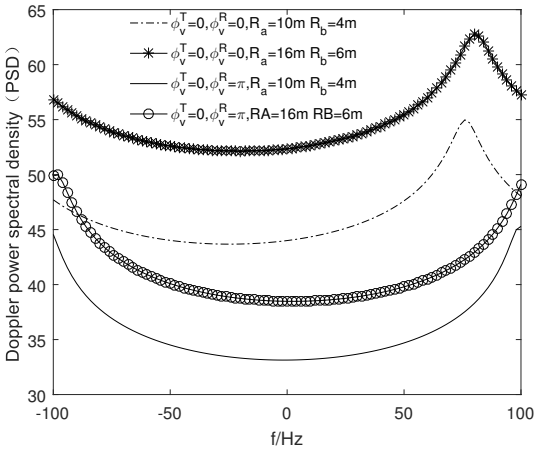

(**a**)

Figure 10. DPSD of SET and without ceiling. (**a**) DPSD of SET. (**b**) DPSD of SET without ceiling.

5.2. Channels of RT and RT with Arched Ceiling

Figures 11 and 12 show the absolute values of the space CCFs of the LoS and NLoS propagation links. It can be found that when we set the antenna element spacing as $\delta_T = \delta_R = 0$, the spatial correlation between the two elements of conventional RT is larger than that of RT with arched ceiling. Moreover, when the element spacing increases, the SCCF gradually attenuates and fluctuates in stable states. Compared with Figure 11, SCCF fluctuates above 0.4, indicating that the correlation can be reduced by increasing the element spacing or adjusting the tunnel communication scenarios.

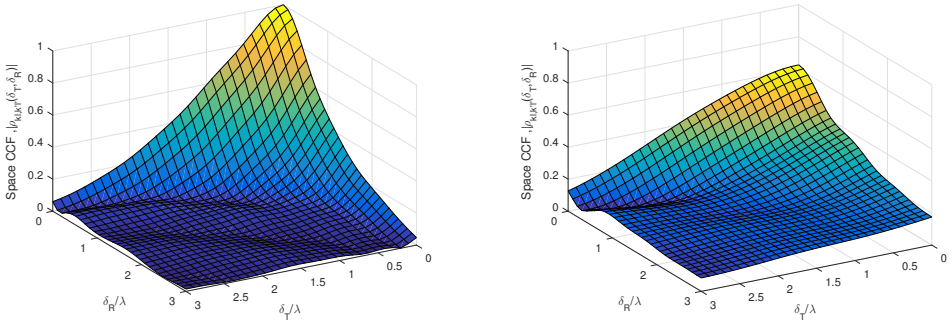

(**b**) (**c**)

Figure 11. SCCF of SRT and without ceiling for NLoS scenario ($c_R = 0$). (**a**) SCCF of SRT. (**b**) SCCF of SRT without ceiling.

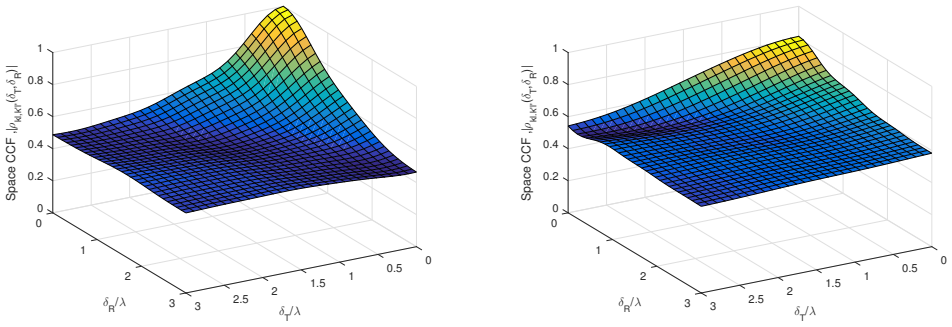

(**a**) (**b**)

Figure 12. SCCF of SRT and without ceiling for NLoS scenario ($c_R = 1$). (**a**) SCCF of SRT. (**b**) SCCF of SRT without ceiling.

In Figure 13, the impacts of the Rice distribution factor on the temporal ACFs of the propagation links in the proposed V2V channel model for tunnel scenarios are studied. It can be found that when the values of c_R decrease, the correlation properties of the propagation links in the time domain increase gradually. Finally, the simulation results of the reference model match with the theoretic results very well.

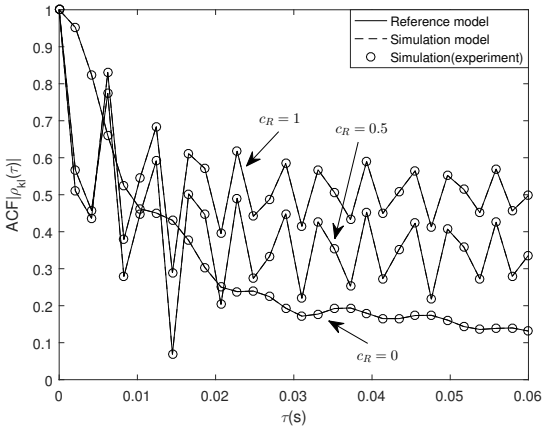

(**a**)

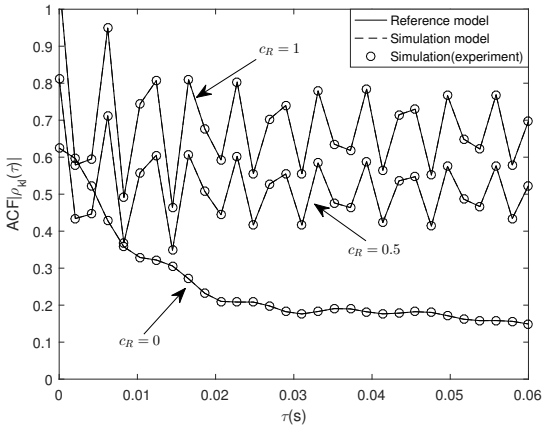

(**b**)

Figure 13. ACF of SRT and without ceiling for NLoS scenario $(c_R = 1)$. (**a**) SCCF of SRT. (**b**) SCCF of SRT without ceiling.

Figure 14 shows the frequency CCFs of the proposed V2V channel model for tunnel scenarios with respect to the different Rician factor. It can be found that the correlation properties of the normal SRT are larger than those of RT with arch ceiling. Furthermore, when we decrease the value of the c_R, the frequency CCFs of the propagation links decay much faster. The simulation results fit very well with the analytical results, which demonstrate the accuracy of the aforementioned discussions.

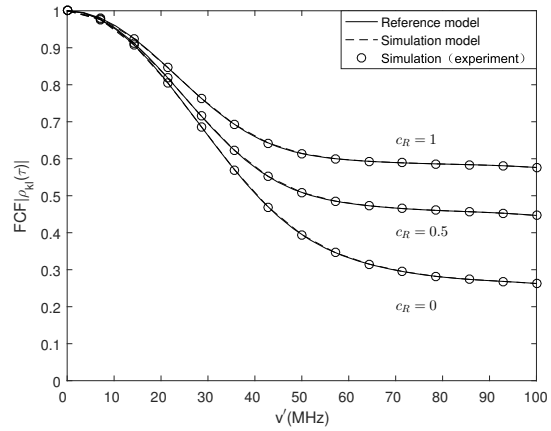

(**a**)

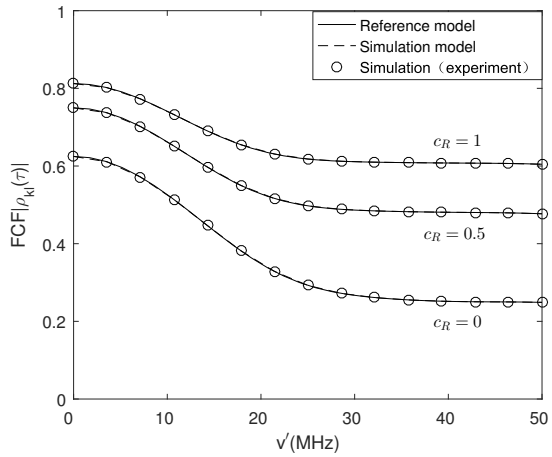

(**b**)

Figure 14. FCF of SRT and without arched ceiling for Rice factors (c_R). (**a**) FCF of SRT. (**b**) FCF of SRT without ceiling.

Figure 15a shows the frequency CCFs of the proposed V2V channel model for tunnel scenarios with respect to the model parameters of the LoS and NLoS propagation links. It can be found that when we increase the value of the cross-sectional width of the tunnel from 8 to 16, i.e., the scattering range increases, the coherence bandwidth decreases from 60 to 40 MHz. In Figure 15b, we notice that the coherence bandwidth decreases gradually as we increase the width.

Figure 16 shows the Doppler PSDs of the proposed V2V channel model for tunnel scenarios with respect to the motion directions of the transmitter and receiver. It can be found that when we increase the height of the tunnel in the proposed V2V channel model, the curves of the Doppler PSDs behave more obviously. Furthermore, when the transmitter and receiver move in the inverse directions, the values of Doppler PSDs increase gradually. Therefore, we can conclude that all the aforementioned results have a great influence on the V2V propagation characteristics for tunnel wireless scenarios.

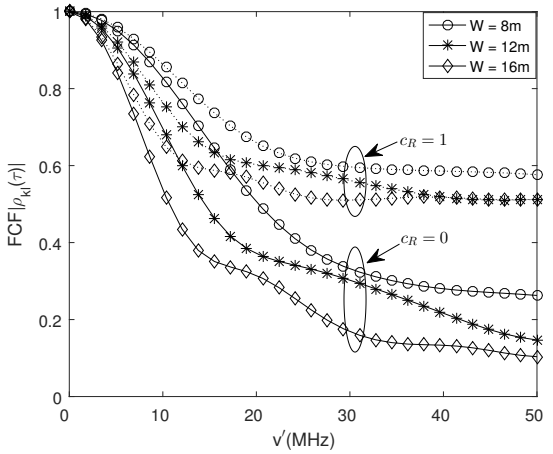

(**a**)

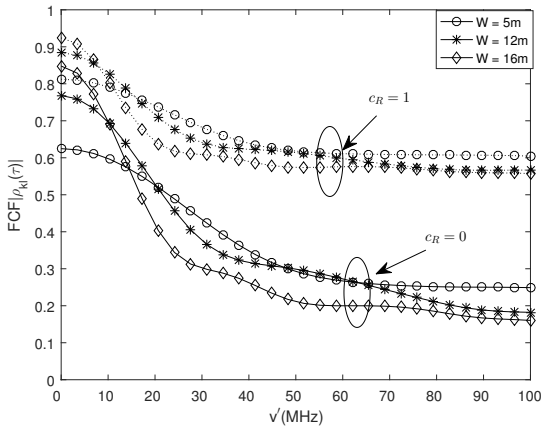

(**b**)

Figure 15. FCF of SRT and without arched ceiling for geometric parameters. (**a**) FCF of SRT (**b**). FCF of SRT without ceiling.

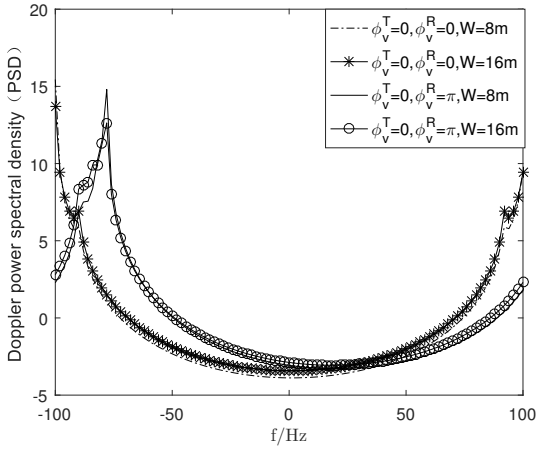

(**a**)

Figure 16. *Cont.*

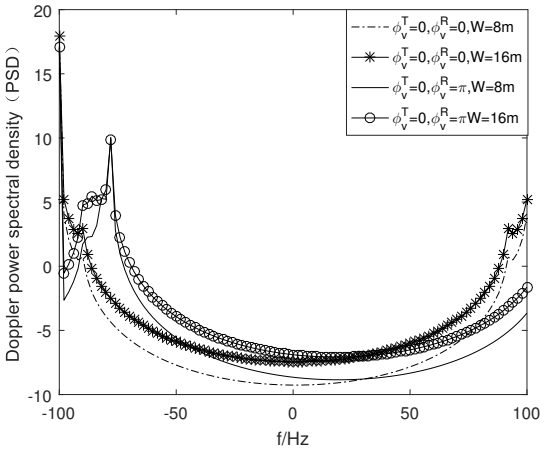

(**a**)

Figure 16. DPSD of SRT and without arched ceiling in various geometrics parameters. (**a**) DPSD of SRT. (**b**) DPSD of SRT without ceiling.

6. Conclusions

In this paper, we have proposed a geometry-based channel model for describing the V2V communications in the practical V2V scenario. The correlation properties, such as the space CCFs, temporal ACFs, frequency CCFs, and Doppler PSDs have been derived and investigated. Numerous simulation results have shown that the propagation characteristics of the proposed V2V channel model are impacted by the physical properties of the tunnel scenarios, the Rician factor, as well as the motion properties of the transmitter and receiver. These observations in principle validate that the proposed modeling solutions are practical for characterizing the propagation characteristics of the V2V channels. As a future work, we can conduct a variety of measurements to further validate the effectiveness of the proposed channel model.

Author Contributions: Data curation, Z.L.; Investigation, H.L.; Methodology, G.S.; Project administration, T.L.; Writing—original draft, S.W.; Writing—review & editing, J.Z. All authors have read and agreed to the published version of the manuscript.

Funding: This research was funded by National Natural Science Foundation of China, grant number 61971167 and 62101274, National Mobile Communications Research Laboratory, Southeast University, grant number 2021D03.

Institutional Review Board Statement: Not applicable.

Informed Consent Statement: Not applicable.

Data Availability Statement: Not applicable.

Conflicts of Interest: The authors declare no conflict of interest. The funders had no role in the design of the study; in the collection, analyses, or interpretation of data; in the writing of the manuscript, or in the decision to publish the results.

References

1. Jiang, H.; Mukherjee, M.; Zhou, J.; Lloret, J. Channel modeling and characteristics analysis for 6G wireless communications. *IEEE Netw.* **2021**, *35*, 296–303. [CrossRef]
2. Wereszczyński, K.; Michalczuk, A.; Paszkuta, M.; Gumiela, J. High-precision voltage measurement for optical Quantum computation. *Energies* **2020**, *15*, 4205 . [CrossRef]
3. Wei, C.; Jiang, H.; Dang, J.; Wu, L.; Zhang, H. Accurate channel estimation for mmWave massive MIMO with partially coherent phase offsets. *IEEE Commun. Lett.* **2022** , 1. [CrossRef]
4. Wang, C.-X.; Huang, J.; Wang, H.; Gao, X.; You, X.-H.; Hao, Y. 6G wireless channel measurements and models: Trends and challenges. *IEEE Veh. Technol. Mag.* **2020**, *15* , 22–32. [CrossRef]

5. Jiang, H.; Ying, W.; Zhou, J.; Shao, G. A 3D wideband two-cluster channel model for massive MIMO vehicle-to-vehicle communications in semi-ellipsoid environments. *IEEE Access* **2020**, *8*, 23594–23600. [CrossRef]
6. Wang, C.-X.; Bian, J.; Sun, J.; Zhang, W.; Zhang, M. A survey of 5G channel measurements and models. *IEEE Commun. Surveys Tuts.* **2018**, *20*, 3142–3168. [CrossRef]
7. Zhang, J.; Pan, C.; Pei, F.; Liu, G.; Cheng, X. Three-dimensional fading channel models: A survey of elevation angle research. *IEEE Commun. Mag.* **2014**, *52*, 218–226. [CrossRef]
8. Jiang, H.; Zhou, J.; Hisakazu, K. Angle and time of arrival statistics for a 3-D pie-cellular-cut scattering channel model. *Wirel. Personal Commun.* **2014**, *78*, 851–865.
9. Jiang, H.; Zhang, Z.C.; Wu, L.; Dang, J.; Gui, G. A 3-D non-stationary wideband geometry-based channel model for MIMO vehicle-to-vehicle communications in tunnel environments. *IEEE Trans. Veh. Technol.* **2019**, *68*, 6257–6271. [CrossRef]
10. Yuan, Y.; Wang, C.; He, Y.; Alwakeel, M.M.; Aggoune, E.M. 3D wideband non-stationary geometry-based stochastic models for non-isotropic MIMO vehicle-to-vehicle channels. *IEEE Trans. Wirel. Commun.* **2015**, *14*, 6883–6895. [CrossRef]
11. Jiang, H.; Zhang, Z.; Wu, L.; Dang, J. Novel 3-D irregular-shaped geometry-based channel modeling for semi-ellipsoid vehicle-to-vehicle scattering environments. *IEEE Wirel. Commun. Lett.* **2018**, *7*, 836–839. [CrossRef]
12. Jiang, H.; Zhang, Z.C.; Dang, J.; Wu, L. Analysis of geometric multi-bounced virtual scattering channel model for dense urban street environments. *IEEE Trans. Veh. Technol.* **2017**, *66*, 1903–1912. [CrossRef]
13. Zhang, J.; Liu, L.; Han, B.; Li, Z.; Zhou, T.; Wang, K.; Wang, D.; Ai, B. Concepts on train-to-ground wireless communication system for hyperloop: Channel, network architecture, and resource management. *Energies* **2020**, *13*, 4309. [CrossRef]
14. Ching, G.S.; Ghoraishi, M.L.; Mann, M.; Lertsirisopon, N.; Takada, J.I.; Imai, T.; Sameda, I.; Sakamoto, H. Wideband polarimetric directional propagation channel analysis inside an arched tunnel. *IEEE Trans. Antennas Propag.* **2009**, *57*, 760–767. [CrossRef]
15. Liu, Y.; Wang, C.X.; Huang, J.; Sun, J.; Zhang, W. Novel 3-D nonstationary mmWave massive MIMO channel models for 5G high-speed train wireless communications. *IEEE Trans. Veh. Technol.* **2019**, *68*, 2077–2086. [CrossRef]
16. Zhou, J.; Wang, X.; Jiang, H.; Sasaki, S.; Shao, G. MIMO channel estimation with arbitrary angle of arrival incident power spectrum for wireless communications. *IET Commun.* **2020**, *15*, 232–244. [CrossRef]
17. Fayziyev, A.; Patzold, M.; Masson, E.; Cocheril, Y.; Berbineau, M. A measurement-based channel model for vehicular communications in tunnels. In Proceedings of the IEEE WCNC, Istanbul, Turkey, 6–9 May 2014; pp. 116–121.
18. Jiang, S.; Song, J.; Wang, W.; Ibrahim, R. A study on radio propagation channel modelling for tunnels. In Proceedings of the EuCAP, Madrid, Spain, 27 March–1 April 2022; pp. 1–4.
19. Avazov, N.; Patzold, M. A novel wideband MIMO car-to-car channel model based on a geometrical semi-circular tunnel scattering model. *IEEE Trans. Veh. Technol.* **2016**, *65*, 1070–1082. [CrossRef]
20. He, R.; Ai, B.; Stuber, G.L.; Zhong, Z. Mobility model-based non-stationary mobile-to-mobile channel modeling. *IEEE Trans. Wirel. Commun.* **2018**, *17*, 4388–4400. [CrossRef]
21. Jiang, H.; Chen, Z.; Zhou, J.; Dang, J.; Wu, L. A general 3D non-stationary wideband twin-cluster channel model for 5G V2V tunnel communication environments. *IEEE Access* **2019**, *7*, 137744–137751. [CrossRef]
22. Li, Y.; He, R.; Lin, S.; Guan, K.; He, D.; Wang, Q.; Zhong, Z. Cluster-based nonstationary channel modeling for vehicle-to-vehicle communications. *IEEE Antennas Wirel. Prop. Lett.* **2017**, *16*, 1419–1422. [CrossRef]
23. Ghazal, A.; Yuan, Y.; Wang, C.X.; Zhang, Y.; Yao, Q.; Zhou, H.; Duan, W. A non-stationary IMT-Advanced MIMO channel model for high-mobility wireless communication systems. *IEEE Trans. Wirel. Commun.* **2017**, *16*, 2057–2068. [CrossRef]
24. Ghazal, A.; Wang, C.-X.; Ai, B.; Yuan, D.; Haas, H. A nonstationary wideband MIMO channel model for high-mobility intelligent transportation systems. *IEEE Trans. Intel. Transp. Syst.* **2015**, *16*, 885–897. [CrossRef]
25. Jiang, H.; Xiong, B.; Zhang, Z.; Zhang, J.; Zhang, H.; Dang, J.; Wu, L. Novel statistical wideband MIMO V2V channel modeling using Unitary matrix transformation algorithm. *IEEE Trans. Wirel. Commun.* **2021**, *20*, 4947–4961. [CrossRef]
26. Xiong, B.; Zhang, Z.; Zhang, J.; Jiang, H.; Dang, J.; Wu, L. Novel multi-mobility V2X channel model in the presence of randomly moving clusters. *IEEE Trans. Wirel. Commun.* **2021**, *20*, 3180–3195. [CrossRef]
27. Xiong, B.; Zhang, Z.; Jiang, H.; Zhang, J.; Wu, L.; Dang, J. A 3D non-stationary MIMO channel model for reconfigurable intelligent surface auxiliary UAV-to-ground mmWave communications. *IEEE Trans. Wirel. Commun.* **2022** , *21* , 5658–5672 . https://doi.org.10.1109/TWC.2022.3142437. [CrossRef]
28. Xiong, B.; Zhang, Z.; Jiang, H.; Zhang, H.; Zhang, J.; Wu, L.; Dang, J. A statistical MIMO channel model for reconfigurable intelligent surface assisted wireless communications. *IEEE Trans. Commun.* **2022**, *70*, 1360–1375. [CrossRef]
29. Jiang, H.; Ruan, C.; Zhang, Z.; Dang, J.; Wu, L.; Mukherjee, M.; da Costa, D.B. A general wideband non-stationary stochastic channel model for intelligent reflecting surface-assisted MIMO communications. *IEEE Trans. Wirel. Commun.* **2021**, *20*, 5314–5328. [CrossRef]
30. Payami, S.; Tufvesson, F. Channel measurements and analysis for very large array systems at 2.6 GHz. In Proceedings of the EUCAP, Prague, Czech Republic, 22–26 March 2012; pp. 433–437.